

# Development and tribological studies of a novel metal-ceramic hybrid brake disc

Thorsten Opel  | Nico Langhof | Walter Krenkel

Department of Ceramic Materials  
Engineering, University of Bayreuth,  
Germany

## Correspondence

Thorsten Opel, Department of Ceramic  
Materials Engineering, University of  
Bayreuth, Germany.  
Email: Thorsten.Opel@uni-bayreuth.de

## Abstract

Ceramic matrix composite (CMC) friction materials show promising tribological properties. Typically, carbon ceramic brake discs consist of a C/SiC rotor which is joined to a brake disc bell. Within this work, a novel metal-ceramic hybrid brake disc, consisting of C/SiC friction segments which are mounted by screws onto an aluminum carrier body, was designed and investigated. A prototype was built which was tribologically tested with three different brake pad materials, LowMet reference, modified SF C/SiC as well as C/C. A constant starting sliding velocity of 20 m/s and braking pressures of 1, 2, and 3 MPa were investigated. To simulate emergency braking conditions 10 consecutive brake applications were carried out in close succession for each brake pad material and braking pressure. The C/C brake pad material showed the highest average coefficient of friction followed by the LowMet and C/SiC material. However, the wear rates of the C/C and LowMet material were orders of magnitude higher compared to the C/SiC material.

## KEYWORDS

ceramic engineering, ceramic matrix composites, silicon carbide, wear/wear resistance

## 1 | INTRODUCTION

Carbon ceramic C/SiC friction materials were developed in the 1990s at the German Aerospace Research Centre (DLR) in Stuttgart<sup>1–5</sup> and are state of the art for performance sports cars and luxury sedans. They show desirable properties, like low density (<2 g/cm<sup>3</sup>), exceptional tribological properties, damage tolerance and have been a focus of research.<sup>6–16</sup> Apart from organic brake pads, the tribological properties of different materials like, for example, C/SiC,<sup>9,11,12,17–20</sup> sintered metallics (MMC),<sup>15,21–25</sup> ceramics<sup>26</sup> and metals<sup>22,26,27</sup> have been investigated against C/SiC.

Krenkel<sup>5</sup> reported coefficient of friction (COF) values between 0.4 and 0.5 for organic brake pads on a SiCralee coated C/SiC brake disc. Langhof et al.<sup>11</sup> tested LowMet and short-fiber reinforced C/SiC brake pads against a full-scale C/SiC brake disc and found COF values of 0.2–0.42 for LowMet and 0.24–0.64 for SF C/SiC brake pads. Li&Yan<sup>12</sup> compared the

tribological properties of C/C, C/SiC and metallic brake pads on a high-density C/SiC brake disc, where C/SiC showed a COF in the range of 0.34–0.44, C/C in-between 0.22–0.24 and the metallic brake pads were reported with a COF of 0.30–0.32.

Apart from the exceptional tribological performance of C/SiC brake discs, they show remarkable wear resistance.<sup>5,9</sup> However, due to the very high manufacturing costs of C/SiC brake discs, this technology is focused on high priced sports cars and luxury sedans. A broader use of this technology, for example, in trains, lorries or low to mid-priced sedans could not be achieved over the past 20 years.

In this study, a new metal-ceramic hybrid brake disc concept is presented, which allows to reduce the amount of C/SiC material needed for the manufacturing of a brake disc significantly. A prototype was designed using computer aided design (CAD) and finite element analysis (FEA) techniques, which consists of thin short-fiber reinforced C/SiC friction segments which were screwed onto an aluminum carrier body. A prototype

metal-ceramic hybrid brake disc with an outer diameter of 410 mm was manufactured and tested on a lab scale dynamometer under emergency braking conditions. Three different brake pads materials (LowMet, C/C and C/SiC) were studied at a start sliding velocity of 20 m/s and three different braking pressures of 1, 2, and 3 MPa. Furthermore, the temperatures of the brake disc after each brake application as well as the wear rates of the brake pads and C/SiC frictions segments of the hybrid brake disc were discussed and summarized.

## 2 | EXPERIMENTAL PROCEDURES

### 2.1 | Raw materials

#### 2.1.1 | Aluminum carrier body

Several aluminum alloys were considered for the carrier body which was milled out of a rod made of the forgeable alloy 2618A/3.1924T851 (AlCu2Mg1.5Ni). This alloy was used because of its high yield strength at room temperature (395 MPa) and at elevated temperatures (220 MPa at 260°C).

#### 2.1.2 | Friction segments

For the friction segments and ceramic brake pads a short carbon fiber-reinforced SiC (C/SiC) was used, which was processed entirely in house. The short fibers (Tenax HTA 40, 3K, Teijin K.K.) were cut to a length of 12 mm and mixed with phenolic resin (Bakelite® FP 6109, Hexion Inc.). The fiber volume content of the resulting CFRP was set to about 35 vol.-%. The fiber resin mixture was warm pressed at 170°C and tempered at 300°C. For the ceramization of the resulting green bodies the liquid silicon infiltration process (LSI process) was used, where the green bodies were pyrolyzed at 1000°C, graphitized at 1600°C and finally siliconized at 1600°C.

#### 2.1.3 | Brake pads

As an industry reference brake pad the LowMet “P40-3V” brake pad mixture (Pad A, TMD Friction GmbH) was used,

which is a standard brake pad for carbon ceramic brake discs. A C/SiC brake pad with added friction modifiers developed at our department (Pad B, Ceramic Materials Engineering (CME), University of Bayreuth) was also tested. The matrix consists of phenolic resin and two friction modifiers (10 vol.-% petrol coke: Timrex Timcal PC 40 (Imerys Graphite & Carbon, Swiss) and 5 vol.-% SiC powder: Sika AVR I UF5 (H.C. Stark)) The C/SiC brake pads were sili-conized using the silicon alloy FeSi75 (75 m.-% Si, 25 m.-% Fe; Elkem Bremanger). The finished pads were desiliconized (removal of the residual Si/FeSi) at 1600°C in a crucible with petrol coke granulate. As a third brake pad material a fabric reinforced C/C research material (Pad C, CVT GmbH & Co. KG, Halblech) was investigated. The C/C material was manufactured using the chemical vapor infiltration method. SiC powder was added to the fiber preform prior to infiltration. All investigated brake pads are summarized in Table 1.

### 2.2 | Joining

The ceramic friction segments were screwed onto the carrier body using M10 extra low head cap screws (CBSTS10-14, Misumi). The extra low head allows for thinner friction segments and more wear before the screw heads come in frictional contact, respectively. A torque wrench (Torque Tool 1 – 25, Syntace GmbH) was used to tighten the screws to a torque of 12 Nm.

### 2.3 | Prototype design

The prototype was designed using Autodesk Inventor Professional 2020 (Autodesk) CAD software (Figure 2A). For the FEA Autodesk Nastran In-CAD 2020 (Autodesk) was used.

#### 2.3.1 | Underlying use case

For the design of the metal-ceramic hybrid brake disc prototype, a use case had to be established in which the performance requirements of the brake disc were defined. The

Denomination	Type	Manufacturer	Braking pressures
Pad A	LowMet P40-3V	TMD Friction GmbH, Germany	1, 2, 3 MPa
Pad B	SF reinforced C/SiC, FeSi75, 10 vol.-% PC40, 5 vol.-% SiC	CME, University of Bayreuth	1, 2, 3 MPa
Pad C	C/C Research Material with SiC powder	CVT GmbH & Co. KG, Germany	1, 2, 3 MPa

**TABLE 1** Brake pads used for the tribological testing of the hybrid brake disc prototype

hybrid brake disc should be able to withstand at least one emergency brake application of a battery electric vehicle (BEV) with a mass of 1.8 t from 200 km/h to 0 km/h at the front axle (highest braking loads, about 1/3 of braking energy are dissipated per front axle brake disc). After such an emergency brake application the brake disc will need to cool down. This consideration follows as a full frictional braking event from 200 km/h implies a severe problem with the electric drive train or the electric motors, respectively. Thus, such an assumption can be made to further enhance potential weight savings.

Considering the use in a BEV the brake disc will also have to function in tandem with the recuperative brake (blending mode). Furthermore, the prototype was designed with the dynamometer of the University of Bayreuth (UBT) in mind, which is limited in its max rpm while operating with the 800 kg flywheel (see 2.5.1). Therefore, the friction radius was set to 184 mm to ensure the friction velocities translate to real life situations. Additionally, the joining method of the friction segments onto the aluminum was fixed to screwing. This was as a result of considerations regarding the longevity of the prototype. Screwing the segments onto the carrier body ensures an easy exchangeability of the friction segments in case of a failure of a single friction segment.

### 2.3.2 | Mechanical calculation and simulation

The mechanical calculation was conducted using FEA, where the resulting brake forces of the use case:  $F_{\text{braking}} = 11\,131\text{ N}$  ( $a = -10\text{ m/s}^2$ ;  $r_{\text{friction}} = 184\text{ mm}$ ;  $r_{\text{tire}} = 341.35\text{ mm}$  (corresponds to tire type 205–55–18)) was split onto the three corresponding friction segments pockets on both sides of the hybrid brake disc (theoretical 30% overlap of the brake pads). A fixed type constraint was used at the 10 fastening holes. Rotational forces (26 rev/sec) were also incorporated in the FEA model.

### 2.3.3 | Thermal simulation

To keep the thermal simulation as simple as possible, a worst-case approach was pursued encompassing some simplifications. The braking event was modelled as a heat flux into the friction surface of the friction segments. Heat losses during and after the braking event in form of heat radiation or convection were not taken into account. Also, the heat flux into the brake pads during a braking event as well as the aerodynamic drag of the car were not considered in the thermal FEA.

As a result, one third of the kinetic energy of the car ( $E_{\text{kin,FA}} \approx 0.93\text{ MJ}$ ) brake disc at the front axle) is flowing into

the friction segments surface in the form of thermal energy during the simulation. To calculate the value of the heat flux, the braking time is calculated with a constant deceleration of  $10\text{ m/s}^2$ , resulting in a braking time of approximately 5.5 s and a resulting heat flux of 169.09 kW. For the FEA, the heat flux density has to be calculated using the friction surface area of the 22 friction segments ( $A_{\text{segment}} = 2519.62\text{ mm}^2$ ), resulting in a heat flux density of  $3.05\text{ W/mm}^2$ . The surface contacts were modelled as bonded. The material data is shown in Table 2. As a simplification the thermal conductivity of the short fiber reinforced C/SiC was modelled isotropic, because the conductivity in thickness direction is the critical value for the temperature of the aluminum carrier body. Furthermore, the differing in-plane thermal conductivity values can be neglected, because the heat flux is modelled as a homogeneous heat flux into the whole friction surface.

## 2.4 | Prototype fabrication

The final design of the hybrid brake disc was manufactured at the UBT workshop. The aluminum carrier body was milled, the short fiber reinforced C/SiC friction segments were processed at the department (CME) using the LSI process and afterward the contours were spark eroded and the surfaces, chamfers as well as the screw seats were ground.

## 2.5 | Tribological testing

### 2.5.1 | Dynamometer of the University of Bayreuth

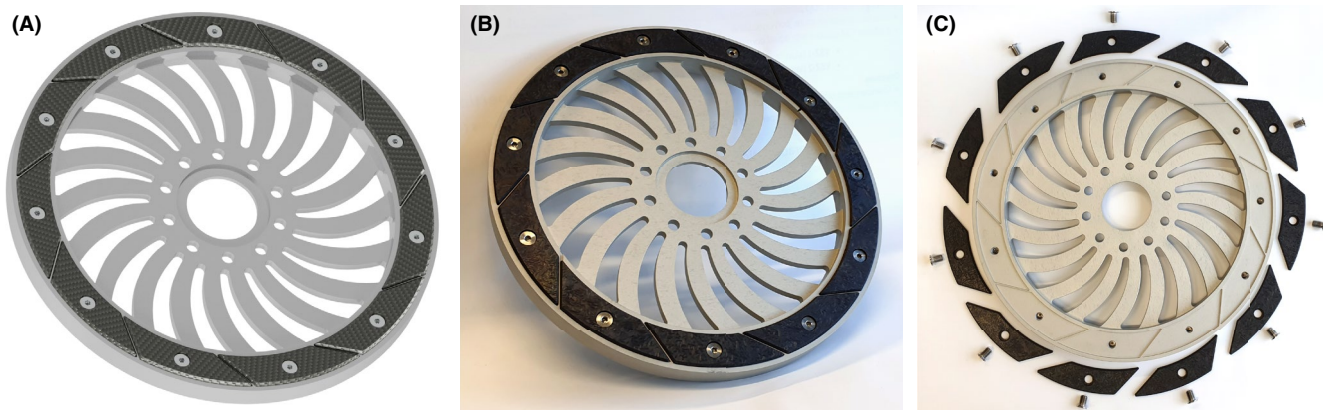
The prototype brake disc was tested on the dynamometer brake test stand of the UBT. An overview of the dynamometer test setup can be seen in Figure 1. The brake test stand contains of an electric motor (45 kW), a fly wheel (different masses/inertias possible), a flange with different adapters for different kinds of brake discs as well as a brake calliper which is pneumatically actuated. All tribological tests in this paper were performed with an 800 kg fly wheel (inertia =  $96\text{ kgm}^2$ ).

TABLE 2 Material data used for the thermal simulation of the hybrid brake disc

	Al carrier body	C/SiC friction seg.	Steel screws
Density [g/cm <sup>3</sup> ]	2.8	2.0	8.0
Heat capacity [J/gK]	0.9	1.2	0.5
Thermal conductivity [W/mK]	150.0	5.0	16.2



**FIGURE 1** (A) Dynamometer test setup with hybrid brake disc, fly wheel, electric motor, and brake calliper, (B) hybrid brake disc during a tribological test run (brake application 10 of 10)



**FIGURE 2** Final design of the metal-ceramic hybrid brake disc (outer diameter = 410 mm): (A) rendering of CAD-Design, (B) photo of the built prototype, (C) carrier body with friction segments and correspondent screws

### 2.5.2 | Hybrid brake disc testing

The metal-ceramic hybrid brake disc prototype was tested (Figure 1B) with different brake pads, as can be seen in Table 1. The size of the brake pads was  $30 \times 30 \times 10 \text{ mm}^3$ . They were tested with three different braking pressures of 1, 2, and 3 MPa. Every test run consisted of 10 consecutive brake applications from a start sliding velocity of 20 m/s to 0 m/s which equates to a braking energy of about 0.54 MJ. After each test run, the friction surface of the friction segments of the hybrid brake disc was cleaned using acetone. The friction radius of 184 mm was kept constant for all test runs.

The wear of the brake pads was determined both by weight loss ( $[\text{mg}/\text{MJ}]$ ) and thickness loss ( $[\text{mm}^3/\text{MJ}]$ ) after every test run. The friction segments of the hybrid brake discs were weighted before the tribological testing and after the whole

tribological testing was finished resulting in a total wear rate after all conducted test runs. Furthermore, the temperature of the hybrid brake disc was determined with an infrared pyrometer (Laserliner CondenseSpot, UMAREX GmbH & Co. KG,  $\varepsilon = 0.95$ ) at four different locations (Figure 5C) after each brake application at the start of the ramp up for the next brake application. The ramp up of the motor/flywheel in between the consecutive brake applications took about 70 s each time.

### 2.5.3 | Brake pad friction surface examination

After the tribological tests were conducted the friction surfaces of the brake pads were examined using a scanning electron microscope (SEM) (Sigma 300 VP, Carl Zeiss AG). Before the friction surfaces were analyzed they were sputtered with a thin gold coating to avoid surface charges.

### 2.5.4 | Friction segment surface examination

To characterize the main wear mechanisms of the metal-ceramic brake disc. The surface of the friction segments of the hybrid brake disc was analysed using a SEM before and after conducting all tribological test runs.

## 3 | RESULTS

### 3.1 | Prototype design

The final design of the metal-ceramic hybrid brake disc prototype can be seen in Figure 2. Eleven C/SiC friction segments are mounted inside milled pockets onto each side of the aluminum carrier body with one flat head screw each. The thickness of the outer ring of the carrier body is 25 mm, the depth of the milled pockets equals 2 mm. At the vanes, the thickness equals 9 mm. The C/SiC friction segments have a thickness of 5 mm. In total, the prototype's mass sums up to ca. 4.8 kg (aluminum carrier body:  $\approx 3.94$  kg, C/SiC segments:  $\approx 0.66$  kg, screws:  $\approx 0.2$  kg).

#### 3.1.1 | Special considerations

The segmentation of the ceramic friction surface is a result of economic considerations. The manufacturing of big C/SiC friction rings is a lot more cost-intensive than the production of the much smaller friction segments. Furthermore, the CFRP green bodies of the segments could be manufactured in a continuous manner using pultrusion techniques, which is also more cost effective.

Due to the use of C/SiC friction segments on an aluminum carrier body some special considerations had to be taken into consideration during the design of the prototype. The transmission of the friction forces from the C/SiC friction segments into the aluminum carrier body should not be done through bearing stresses in the drill holes of the screw seats, because this is inadequate for ceramic materials because of developing stress peaks inside the ceramic material which can result in a potential material failure. To counteract this effect, the friction segments are fitted into milled pockets with fillets in between the different segments. The holes of the screw seats are deliberately oversized so that the individual screw's only function is the pressing of the correspondent friction segment onto the carrier body—nearly no lateral forces should be transmitted. During a braking event, the friction segments are forced laterally against the fillets of the carrier body which then take up the forces resulting in an area load, which is much more desirable for the CMC material.

For the reduction in COF fluctuations and noise vibration harshness phenomena (NVH) the circumferential edges of the

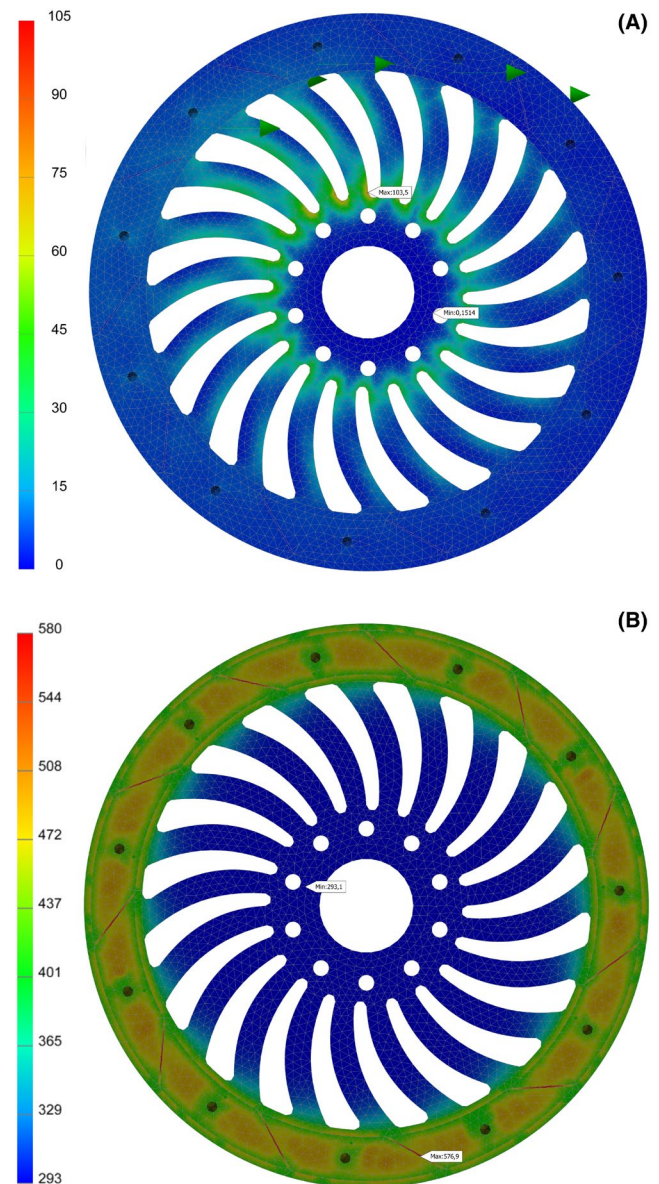


**FIGURE 3** Results of the simulation of the aluminum carrier body: (A) solid von mises stresses [MPa], (B) temperatures [K] 1.25 s after the 5.5 s braking event

friction surface of the friction segments have been chamfered. Furthermore, the fillets as well as the equivalent shape of the friction segments have been angled by  $35^\circ$  to allow a smoother transition of the brake pads from one friction segment to another.

#### 3.1.2 | Finite element analysis

Figure 3A) shows the result of the mechanical simulation of the hybrid brake disc prototype. The maximal stresses can be located at the foot of the vanes near the pitch circle of the mounting holes and amounts to 103.5 MPa.

The results of the thermal simulation of a single braking event can be seen in Figure 3B. Shown is the temperature

distribution in the aluminum carrier body 1.25 s after the 5.5 s braking event, where the maximum temperature of about 300°C (573 K) can be found in the fillet region. The maximum temperature at the friction segment seats is about 210°C (483 K).

### 3.2 | Tribological testing

The measured mean COF of the different brake pads during the individual test runs can be seen in Figure 4. During the 1 and 2 MPa test runs of Pad C, the brake pads were worn out prematurely and the test runs had to be aborted after 9 and 8 consecutive brake applications.

For all tested brake pad materials, a decreasing COF with increasing braking pressure can be found (Figure 4; Table 3). The highest average COF values of 0.90 (1 MPa), 0.76 (2 MPa), and 0.58 (3 MPa) are shown by the C/C-Material (Pad C) followed by 0.73 (1 MPa), 0.60 (2 MPa), and 0.41 (3 MPa) for LowMet (Pad A) and 0.50 (1 MPa), 0.35 (2 MPa), and 0.27 (3 MPa) for C/SiC (Pad B). An increasing COF trend with each brake application at 1 MPa for Pad C and at all braking pressures for Pad A can be seen. The test runs at 2 and 3 MPa for Pad C show a slight increase in the COF at the first three brake applications followed by a slight decrease afterward. The C/SiC brake pad material (Pad B) shows a mostly constant but with increasing brake application number slightly decreasing COF (Figure 4B).

Figure 5 shows the measured temperatures after each brake application for LowMet (Pad A) (A) and C/C (Pad C) (B) brake pads at 3 MPa braking pressure, which showed the highest braking powers. It can be seen that the temperature curves show a limited growth. The temperatures measured for Pad C are slightly higher as for Pad A. The highest temperatures of about 405°C (Pad C) can be measured at the

radial face of the carrier body (T1), followed by the temperature measured at the friction segment surfaces (T2,  $\approx$  380°C, Pad C), carrier body spokes (T3,  $\approx$  220°C, Pad C) and at the flange area (T4,  $\approx$  130°C, Pad C). Furthermore, the measured temperatures are significantly lower than the projected temperatures by the FEA.

The results of the tribological testing of the metal-ceramic hybrid brake disc are summarized in Table 3. Because of the velocity dependence of the COF within single brake applications, the standard deviation seems to be comparatively large. This does not mean, that the mean values of the COF have a great error, but rather, that the COF is more dependent on the velocity and less constant during single brake applications.

It can be seen, that while showing the lowest mean COF values, C/SiC (Pad B) shows the best wear properties (62–93 mg/MJ), where the wear rates are about 85 to 95% lower than the measured wear rates for Pad A and Pad C. The LowMet (Pad A) brake pads show a significant increase of the wear rates with rising braking pressures (547 mg/MJ up to 1874 mg/MJ), whereas the wear rates of the C/C Material seem to fluctuate between 1849 mg/MJ and 2538 mg/MJ.

### 3.3 | Brake pad friction surfaces

The friction surfaces of the LowMet brake pad material (Pad A) after the test runs with 1 MPa and 3 MPa braking pressure can be seen in Figure 6. Only small surface disruptions can be found on the friction surface after the 1 MPa test run (Figure 6, left). After the 3 MPa test run, the friction surface of the brake pad shows major surface disruptions. This effect is also visible in the SEM images (Figure 7), where the friction surface after the 1 MPa test run is smooth and does

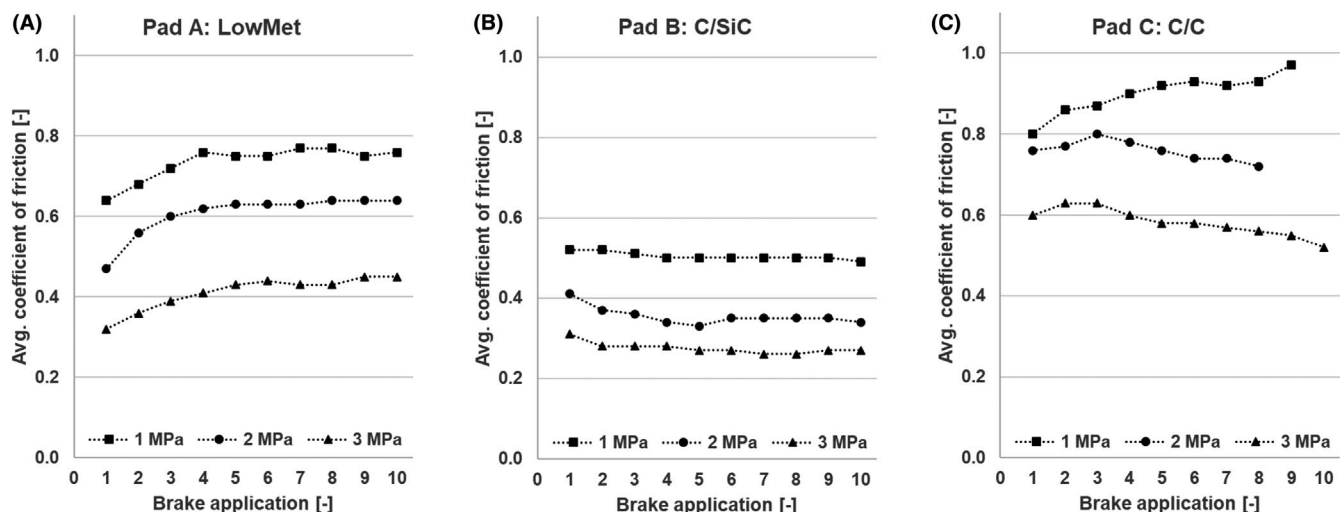


FIGURE 4 Average coefficient of friction of the different test runs at 1, 2 and 3 MPa braking pressure with the hybrid brake disc and (A) Pad A: LowMet, (B) Pad B: C/SiC, (C) Pad C: C/C

TABLE 3 Mean coefficient of friction and wear rates of the different brake pads tested with the metal-ceramic hybrid brake disc

Braking pressure	Pad A: LowMet			Pad B: C/SiC			Pad C: C/C		
	1 MPa	2 MPa	3 MPa	1 MPa	2 MPa	3 MPa	1 MPa	2 MPa	3 MPa
Average COF [-]	0.73 ± 0.13 n = 10	0.60 ± 0.09 n = 10	0.41 ± 0.07 n = 10	0.50 ± 0.16 n = 10	0.35 ± 0.11 n = 10	0.27 ± 0.11 n = 10	0.90 ± 0.15 n = 9	0.76 ± 0.09 n = 8	0.58 ± 0.11 n = 10
Volumetric wear [mm <sup>3</sup> /MJ]	187	348	591	34	49	21	1108	1523	1304
Gravimetric wear [mg/MJ]	547	1169	1874	68	93	62	1849	2538	2188

not show bigger disruptions of the friction film (Figure 7A). In contrast, the surface of the LowMet brake pad (Pad A) after the 3 MPa test run shows massive disruptions (Figure 7B). A brake pad portion with an approximate size of  $0.5 \times 1 \text{ mm}^2$  can be seen which has broken away from the friction surface. The intact friction surface of the 3 MPa specimen seems to be more inhomogeneous compared to the 1 MPa friction surface.

Pad B's friction surface after the 1 MPa test run can be seen in Figure 8. The friction surface shows polished carbon fibers (darker areas) as well as a friction film on as well as in between the carbon fibers. Under higher magnification (Figure 8B) areas with a compact friction film as well as finer debris particles can be identified.

The friction surface of the C/C brake pad material (Pad C) can be seen in Figure 9. In comparison to pad material A & B the friction surface seems to be very smooth, a distinct friction film cannot be identified. Under a higher magnification (Figure 9B) only a few debris particles and no friction film can be identified. Some debris particles seem to plough the brake pad material leaving a trail behind them.

### 3.4 | Friction segment surfaces

The friction surface after the preparation and grinding of the C/SiC friction segments can be seen in Figure 10. The silicon and silicon carbide matrix areas are characterized by the brighter areas, whereas the carbon fibers and carbon matrix areas are represented by the darker areas. It can be seen, that the tips of carbon fibers as well as the surrounding carbon matrix of the different carbon fiber bundles tend to break away during the grinding of the friction segments (Figure 10B), resulting in recessed areas with a rougher surface and exposed carbon fibers (Figure 10C).

Figures 11 and 12 show the friction surface of a C/SiC friction segment after the tribological testing. Carbon as well as Si and SiC matrix areas are still visible. Furthermore, a build-up friction film can be seen primarily in the fiber bundle areas. Similar areas as in Figure 10B can be found on the friction surface of the tribological tested friction segment (Figure 11B). The exposed fibers and surrounding carbon matrix in these areas show clear signs of oxidation, as can be seen using a higher magnification (Figure 12A,B). Neighbouring areas of friction film and Si/SiC matrix do not show signs of oxidation.

### 3.5 | Dismantling and wear of hybrid brake disc

The metal-ceramic hybrid brake disc was tested in over 20 test runs with 215 individual brake applications in total. This sums up to a total of over 115 MJ dissipated braking energy. After the tribological testing the hybrid brake disc could be disassembled without problems. Furthermore, the torque of the

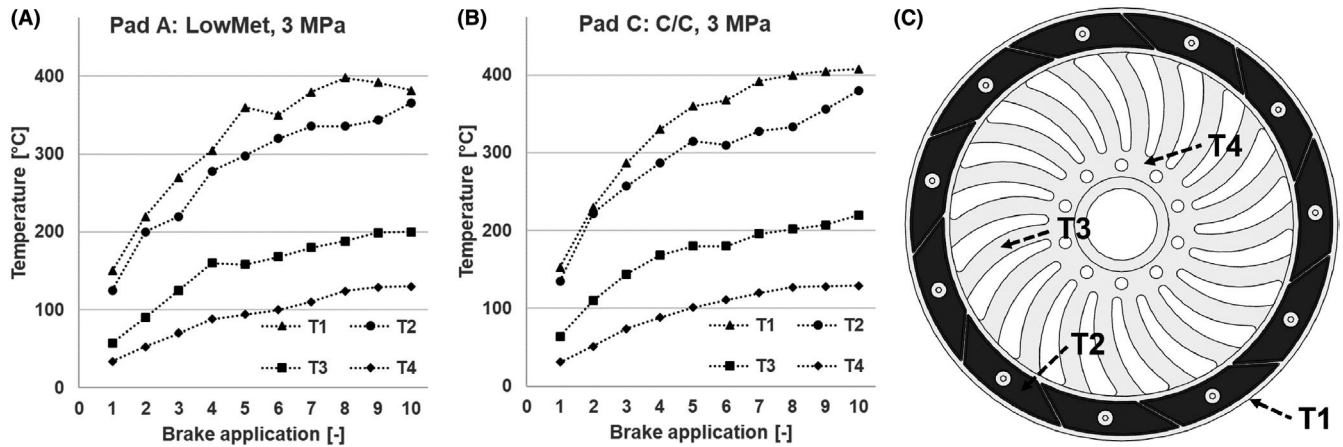


**FIGURE 5** Temperatures of the hybrid brake disc at different locations measured with an infrared pyrometer: (A) Pad A: LowMet, 3 MPa, (B) Pad C: C/C, 3 MPa, (C) locations of the temperature measurements: T1: radial face of carrier body, T2: friction segments surface, T3: middle of carrier body spoke section, T4: flange area of carrier body

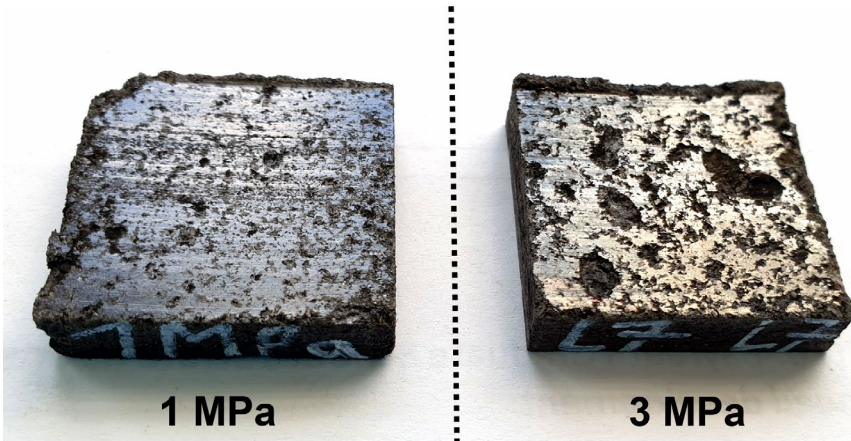


**FIGURE 6** Macrograph of LowMet (Pad A) brake pad (30 × 30 mm<sup>2</sup>) friction surfaces after 1 MPa (left) and 3 MPa (right) test run

screws was checked after each test run, using a torque wrench. However, a loosening or loss of torque of the screws could not be observed. The disassembled hybrid brake disc (Figure 13) shows brake dust under the friction segments. However, the areas around the screw seat seem to be nearly dust free. Figure 13B shows signs of wear of the friction segment surfaces as well as tempering colors of the screw. A thickness loss of the friction segments could not be measured. However, the friction segments showed an average mass loss of about 0.11 g per friction segment. The total mass loss of all friction segments summed up to 2.38 g, resulting in a total measured wear rate of the friction segments over all test runs of 32 mg/MJ.

## 4 | DISCUSSION

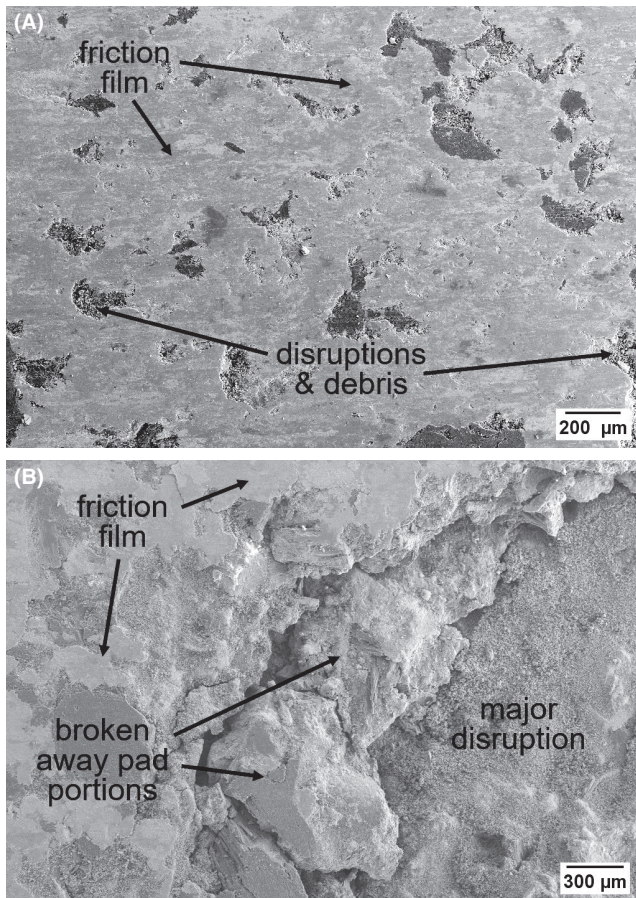
### 4.1 | Thermomechanical simulation of the metal-ceramic hybrid brake disc

The mechanical FEA of the hybrid brake disc showed a maximal stress of 103.5 MPa at the foot of the vanes of the

aluminum carrier body. The used aluminum alloy shows a yield strength of 395 MPa at room temperature and 220 MPa at 260°C. This means a safety factor near 4 at room temperature and over 2 above 260°C can be achieved. As can be seen the calculated (Figure 3B) and measured temperatures (Figure 5) at the points where the maximum stresses occur are well beyond 260°C, which means a safety factor of well above 2 could be achieved.

The measured temperatures during the tribological testing (Figure 5) are far below the calculated temperatures. On the one hand, the maximal energy of one braking event on the dynamometer is smaller (dynamometer: 0,54 MJ, simulation/use case: 0,93 MJ). On the other hand, cooling effects like convection, thermal radiation, and the heat flow into the brake pads were disregarded for the thermal FEA.

After three subsequent brake applications the measured temperatures in the aluminum carrier body rises over 250°C which can result in a softening of the used precipitation hardened alloy. However, the temperatures at the load bearing region near the flange (T4) and at the middle of the vane area (T3) reach a maximum of 220°C (Pad C,



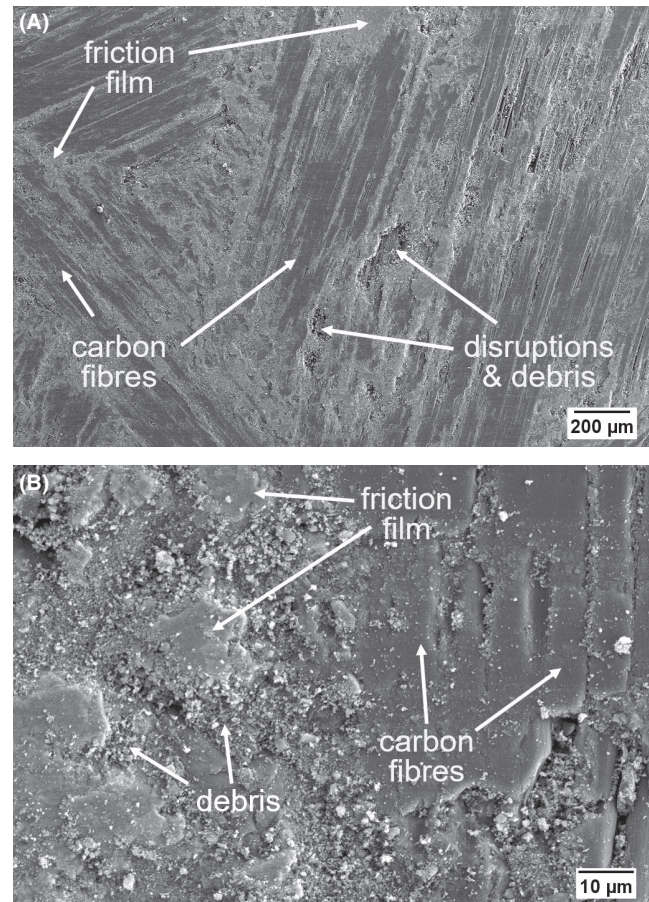
**FIGURE 7** SEM pictures of LowMet (Pad A) brake pad friction surfaces: (A) after 1 MPa test run (magnification: 50 $\times$ ), (B) after 3 MPa test run (magnification: 35 $\times$ )

Figure 5B) after 10 brake applications in direct succession, which means a sufficient safety factor of over 2 could still be realized.

## 4.2 | Tribological measurements

All tested brake pads showed a decreasing average COF with increasing braking pressure. For C/SiC-C/SiC friction pairings (comparable to Pad B) a decreasing COF with increasing braking pressure was also observed in the literature by Fan et al.<sup>17</sup> who found, that this effect is based on the formation of finer debris particles in the friction film between the brake pads and the brake disc. A rising COF with decreasing braking pressure for organic brake pads (Pad A) can also be found in the literature.<sup>7</sup>

The observed increase in the COF for the first three to four brake applications for pad material A and C is most likely linked to the build-up of a friction film on the brake pad and friction segment surfaces as well as the run in of the friction surface of the brake pads. The decreasing COF after three brake applications at 3 MPa for Pad A and 2 and 3 MPa for



**FIGURE 8** SEM pictures of C/SiC (Pad B) brake pad friction surfaces: (A) after 1 MPa test run (magnification: 50 $\times$ ), (B) after 1 MPa test run (magnification: 1000 $\times$ )

Pad C is probably related to a (thermal/oxidative) degradation of the built-up friction film.

The COF measured for the organic LowMet (Pad A) brake pads at 3 MPa agrees with the literature,<sup>7,11</sup> while the measured COF values for 1 and 2 MPa are slightly higher than the reported values. For the ceramic pad material (Pad B) similar COF values can be found in the literature.<sup>6,10,11,17</sup> A comparable slight decrease in the COF values with rising temperatures/brake applications for C/SiC-C/SiC friction pairings has also been reported in the literature.<sup>6</sup> This effect is most likely linked to the brittle to ductile transition of the free silicon within the C/SiC friction segments. This transition was reported by Hirsch & Roberts<sup>28</sup> and is starting around 500–550°C. The friction segments showed red heat during the test runs (Figure 1B), which means the threshold temperature of around 500 – 550°C is well exceeded. Due to the ductile deformation behaviour of silicon above this temperature, it is probable that fewer particles brake out from the friction surface, resulting in a lesser pronounced mechanical interlocking of the friction surfaces. Ultimately, the decrease of mechanical interlocking between the friction surfaces of

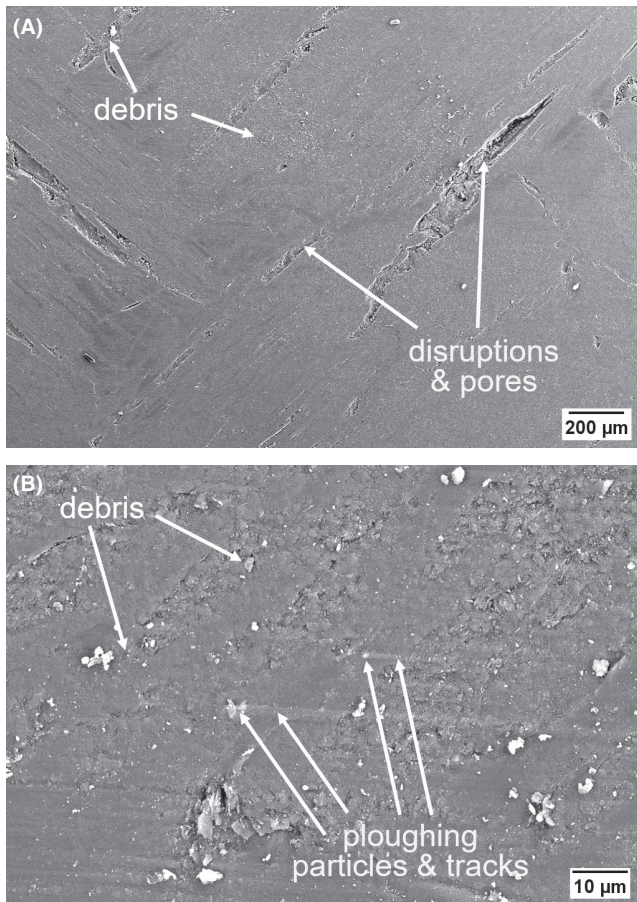


**FIGURE 9** SEM pictures of C/C (Pad C) brake pad friction surfaces: (A) after 1 MPa test run (magnification: 50 $\times$ ), (B) after 1 MPa test run (magnification: 1000 $\times$ )

the C/SiC-C/SiC friction pairings results in a decreasing COF with rising temperature.

The higher measured wear rates of the LowMet brake pad material (Pad A) compared to literature<sup>11</sup> combined with the increased wear rate with increasing braking pressure, is most likely related to the interrupted friction surface of the metal-ceramic hybrid brake disc. Although the edges of the friction segments are angled and chamfered, to achieve a smooth transition between the different friction segments, due to the compressibility and low stiffness of the LowMet material, the pad material is pressed into the fillet region between the friction segments during braking resulting in a micro shaving and a dynamic shattering of the brake pad material. This effect amplifies with increasing braking pressure which can be seen in the SEM pictures of the friction surface after the 3 MPa test run (Figure 7B).

The wear rates of the ceramic brake pads (Pad B) are comparable to previously reported wear rates for similar friction pairings.<sup>6,10,11</sup> The SEM images showed a dense friction film which seems to adhere to the friction surface, where the spaces between the carbon fibers seem to trap debris particles resulting in the build-up of the friction film. Similar effects

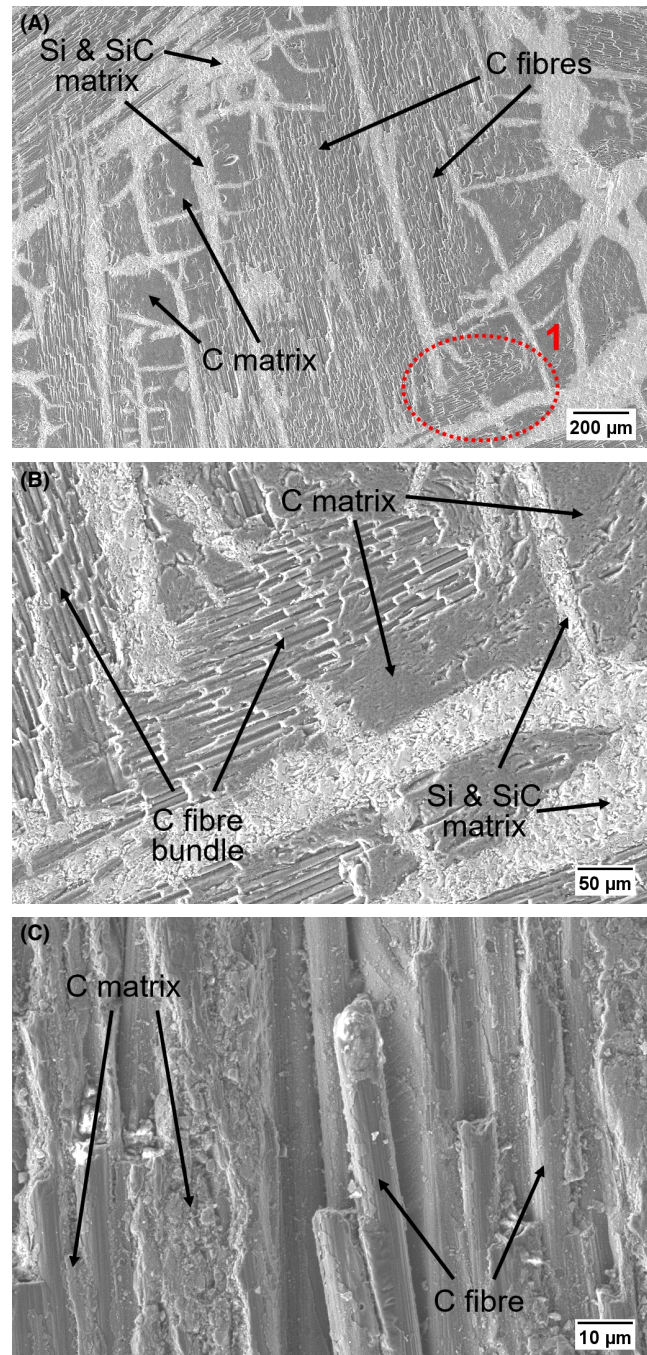


**FIGURE 10** SEM pictures of the friction surface of a C/SiC friction segment of the metal-ceramic hybrid brake disc before tribological testing: (A) overview (magnification: 50 $\times$ ), (B) detailed view of area 1 (magnification: 200 $\times$ ), (C) detailed view of carbon fibers and carbon matrix (magnification: 1000 $\times$ )

were reported in the literature.<sup>11</sup> Due to the low compressibility and the higher stiffness and hardness compared to the LowMet material, a brake pressure induced increase of the wear rate could not be observed for pad material B.

In contrast to the C/SiC brake pad material, the C/C brake pads (Pad C) friction surface showed no build-up of a friction

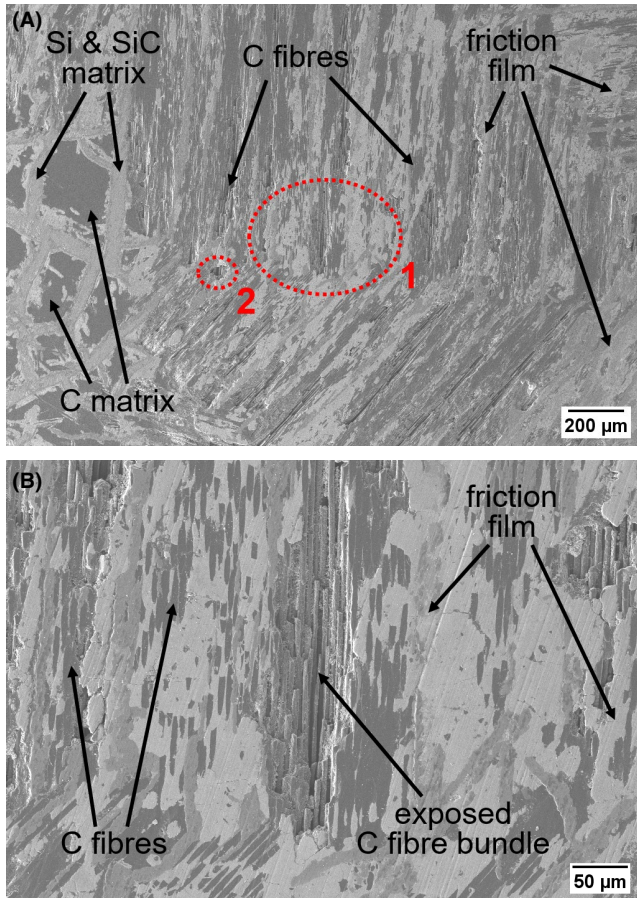


**FIGURE 11** SEM pictures of the friction surface of a C/SiC friction segment of the metal-ceramic hybrid brake disc after tribological testing: (A) overview (magnification: 50 $\times$ ), (B) detailed view of area 1 (magnification: 200 $\times$ )

layer. Smaller debris particles could be observed which seem to plough the relatively soft C/C material. The lack of a stable friction film combined with the observed micro ploughing effect seems to be the reason for the high wear rates compared to pad material B. However, higher wear rates compared to the measured wear rates of the C/C brake pads (Pad C) for C/SiC – C/C friction pairings can be found in the literature.<sup>12,13</sup>

### 4.3 | Dismantling and wear of the metal-ceramic hybrid brake disc

The brake dust that could be found under the friction segments (Figure 13A) indicates, that the friction segments were not resting completely against the carrier body suggesting a lack of contact pressure or rather an uneven distribution of the contact pressure. Hence, one screw could not be sufficient to create an even contact of the friction segments with the carrier body. Additionally, a certain degree of freedom and movement of the friction segments is a part of the design

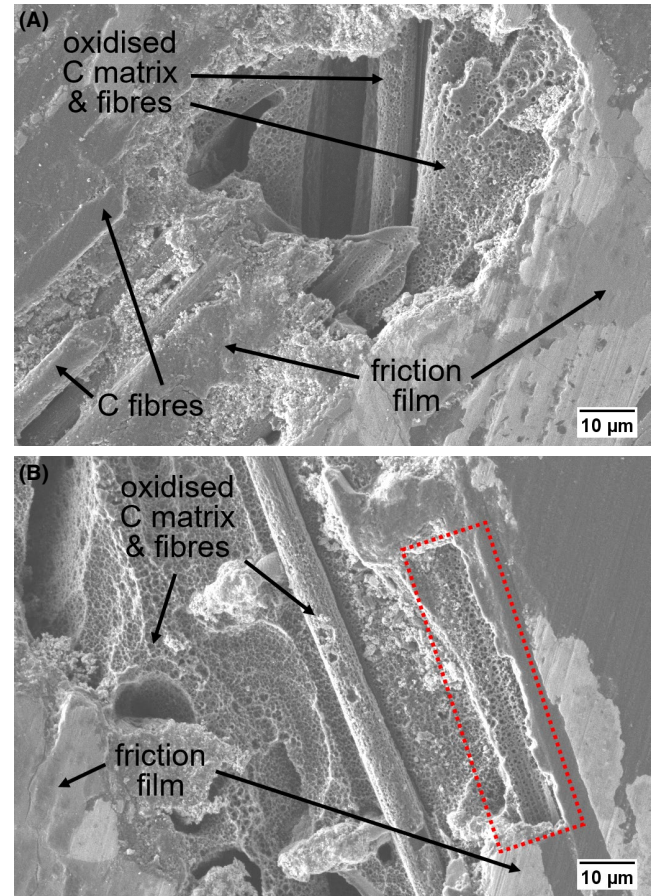


**FIGURE 12** SEM pictures of the friction surface of a C/SiC friction segment of the metal-ceramic hybrid brake disc after tribological testing: (A) detailed view of area 2 of Figure 11A (magnification: 1000 $\times$ ), (B) detailed view of oxidised carbon fiber and carbon matrix (magnification: 1000 $\times$ )

of the metal-ceramic hybrid brake disc to achieve a ceramic friendly fixing of the friction segments (as stated in 3.1.1), which could also attribute to a brake dust migration under the friction segments. Wear at the backside of the friction segments or at the surface of the carrier body could not be observed.

Wear rates reported for C/SiC brake discs without a SiC friction surface can be found in the literature<sup>6,10</sup> and are higher than the wear rate measured for the friction segments. The SEM images of the tribological tested friction segment showed clear signs of oxidation of the carbon fibers as well as of the surrounding carbon matrix areas (Figures 11 and 12). Oxidation of carbon starts at about 400 $^{\circ}$ C, which is in the region of the measured temperatures of the carrier body and friction segments. During the braking event, the friction surface of the brake disc is heated well above the 400 $^{\circ}$ C threshold as the frictions surface shows red heat during tribological testing. The oxidation products of carbon are CO and CO<sub>2</sub>. Because of their gaseous nature, a negative impact of

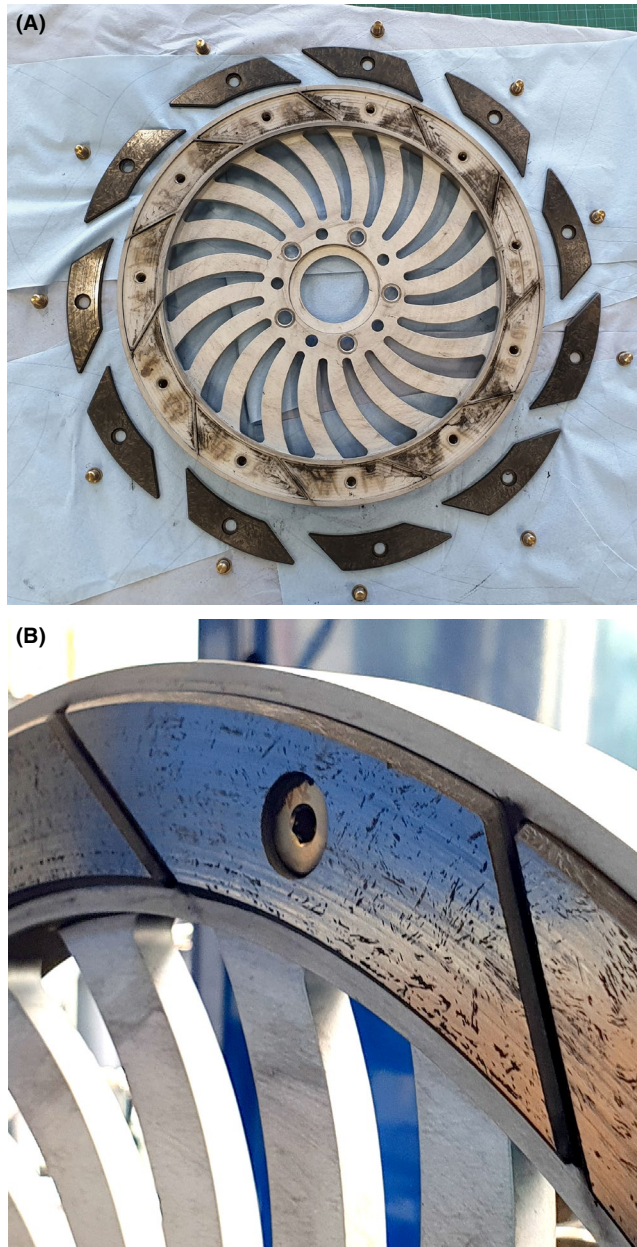


**FIGURE 13** Disassembly and wear of the metal-ceramic hybrid brake disc (outer diameter = 410 mm): (A) Disassembled hybrid brake disc with friction segments and screws, (B) Friction surface of a friction segment with first visible signs of wear

the oxidation products on the tribological performance of the hybrid brake disc is highly unlikely.

A thickness loss of the friction segments could not be measured, which means the abrasive wear seems to be sufficiently small to be negligible. Furthermore, the friction surface showed areas with a dense friction film as well as Si and SiC matrix areas, which didn't show any signs oxidation. Hence, the wear of the friction segments can be primarily attributed to oxidative wear of the carbon fibers

as well as the carbon matrix. The areas where this oxidative wear occurs, appear to originate during the grinding process of the friction surface during the manufacturing of the C/SiC friction segments (Figure 10B). The formation of these areas in fiber bundles of C/SiC during grinding by, for example, pull out or truncation is well documented within the literature.<sup>29–31</sup> During braking, these recessed areas are not in frictional contact but are exposed to oxygen and high temperatures resulting in a gradual oxidation of both the carbon fibers and the surrounding carbon matrix. Due to the advancing oxidation these areas tend to grow and can be macroscopically visible over time (Figure 13B). The growth mechanism of these areas can be seen e. g. in Figure 12B, where a segment of a carbon fiber broke away (red highlighted area). Furthermore, a part of the former overlapping friction film is still visible, whereas other parts seem to have already broken away.

## 5 | SUMMARY AND CONCLUSIONS

A metal-ceramic hybrid brake disc consisting of short-fiber reinforced C/SiC friction segments and an aluminum carrier body, was designed using FEA methods, manufactured (total mass: 4.8 kg) and tested with three different brake pad materials (LowMet, C/SiC and C/C) on a dynamometer under emergency braking conditions.

The measured average COF decreased with increasing braking pressure (1, 2, 3 MPa) for every tested brake pad material. C/C showed the highest average COF values (0.58–0.90) followed by LowMet (0.41–0.73) and C/SiC (0.27–0.50). The lowest wear rates were shown by the C/SiC brake pads (62–93 mg/MJ), followed by LowMet (547–1874 mg/MJ) and C/C (1849–2538 mg/MJ). The wear rate of the C/SiC friction segments of the metal-ceramic hybrid brake disc was determined after all test runs and summed up to 32 mg/MJ.

- The metal-ceramic hybrid brake disc is suitable for the outlined use case of braking a 1.8 t car from 200 km/h to 0 km/h.
- The amount of C/SiC material needed for a brake disc could be reduced by one order of magnitude compared to a standard C/SiC brake disc. Regarding the measured temperatures, the mass of the metal-ceramic hybrid brake disc could be reduced considerably, depending on the use case.
- Segmentation of the friction surface and the accompanying fillet regions between the friction segments can result in elevated wear rates of the brake pads. Especially regarding compressible organic brake pads (e. g. LowMet) which showed big disruptions of the friction surface at higher braking pressures as a result of a combined micro shaving and dynamic shattering of the brake pads.

- For automotive applications with a lot of brake applications in blend mode and low braking forces, C/SiC brake pads show the best COF to wear properties.
- If high to very high braking forces are needed, LowMet and C/C brake pads can be used. However, these materials show higher wear rates.
- The wear of the C/SiC friction segments of the metal-ceramic hybrid brake disc seems to be driven by oxidation of the carbon fibers and carbon matrix, starting at carbon fiber bundle areas due to surface defects introduced by surface grinding during the manufacturing of the segments.

## ORCID

Thorsten Opel  <https://orcid.org/0000-0002-0406-6571>

## REFERENCES

- Krenkel W, Henke T. Design of High Performance CMC Brake Discs. In: Kea N, editor. Proc. 3rd Int. Conf. High Temperature Ceramic Matrix Composites (HT-CMC 3), Osaka/Japan, Sept. 6-9, 1998. Trans Tech Pub. Ltd / CH-GE-UK-USA; 1998:421-4.
- Krenkel W. Applications of Fibre Reinforced C/C-SiC Ceramics. Ceramic Forum International. 2003;80:31-8.
- Krenkel W, Berndt F. C/C-SiC composites for space applications and advanced friction systems. Mater Sci Eng, A. 2005;412(1-2):177-81.
- Krenkel W. C/C-SiC Composites for Hot Structures and Advanced Friction Systems. In: Kriven, editor. 27th annual cocoa beach conference on advanced ceramics and composites: B, vol. 24. John Wiley And Sons; 2003. p. 583-92.
- Krenkel W. Carbon fiber reinforced CMC for high-performance structures. Int J Applied Ceramic Technology. 2004;1(2):188-200.
- Krenkel W, Heidenreich B, Renz R. C/C-SiC composites for advanced friction systems. Adv Eng Mater. 2002;4(7):427-36.
- Krenkel W. Carbon fibre reinforced silicon carbide composites (C/SiC, C/C-SiC). In: Bansal NP, editor. Handbook of ceramic composites. New York: Kluwer Academic Publishers; 2005. p. 117-48.
- Krenkel W editor. Ceramic matrix composites: fiber reinforced ceramics and their applications. 1st ed. Weinheim: Wiley-VCH; 2008.
- Krenkel W, Georges TJ. Ceramic matrix composites for friction applications. In: Bansal NP, Lamon J, editors. Ceramic matrix composites: Materials, modeling and technology. Hoboken, New Jersey: John Wiley & Sons, Inc; 2015. p. 647-71.
- Krenkel W, Renz R. CMCs for friction applications. In: Krenkel W, editor. Ceramic matrix composites: fiber reinforced ceramics and their applications. 1st edn. Weinheim: Wiley-VCH; 2008. p. 385-407.
- Langhof N, Rabenstein M, Rosenlöcher J, Hackenschmidt R, Krenkel W, Rieg F. Full-ceramic brake systems for high performance friction applications. J Eur Ceram Soc. 2016;36(15):3823-32.
- Li G, Yan Q. Comparison of friction and wear behavior between C/C, C/C-SiC and metallic composite materials. Tribol Lett. 2015;60(1).
- Xu X, Fan S, Zhang L, Du Y, Cheng L. Tribological behavior of three-dimensional needled carbon/silicon carbide and carbon/carbon brake pair. Tribol Int. 2014;77:7-14.
- Li Z, Xiao P, Xiong X, S-h ZHU. Tribological characteristics of C/C-SiC braking composites under dry and wet conditions. Trans Nonferr Metals Soc China. 2008;18(5):1071-5.
- Ma X, Luan C, Fan S, Deng J, Zhang L, Cheng L. Comparison of braking behaviors between iron- and copper-based powder metallurgy brake pads that used for C/C-SiC disc. Tribol Int. 2021;154:106686.
- Li W, Yang X, Wang S, Xiao J, Hou Q. Research and prospect of ceramics for automotive disc-brakes. Ceram Int. 2021;47(8):10442-63.
- Fan S, Zhang L, Cheng L, Tian G, Yang S. Effect of braking pressure and braking speed on the tribological properties of C/SiC aircraft brake materials. Compos Sci Technol. 2010;70(6):959-65.
- Zhang J, Xu Y, Zhang L, Cheng L. Effect of braking speed on friction and wear behaviors of C/C-SiC composites. Int J Applied Ceramic Technology. 2007;4(5):463-9.
- Zhou X, Zhu D, Xie Q, Luo F, Zhou W. Friction and wear properties of C/C-SiC braking composites. Ceram Int. 2012;38(3):2467-73.
- Li J, Xiao P, Li Z, Zhou P, Chen F, Li Y. Microstructures and tribological behaviors of C f /C-SiC composites tailored by Cu and Fe-Si matrices. Int J Appl Ceram Technol. 2021. <https://doi.org/10.1111/ijac.13703>
- Stadler Z, Krnel K, Kosmac T. Friction behavior of sintered metallic brake pads on a C/C-SiC composite brake disc. J Eur Ceram Soc. 2007;27(2-3):1411-7.
- Bian G, Wu H. Friction and surface fracture of a silicon carbide ceramic brake disc tested against a steel pad. J Eur Ceram Soc. 2015;35(14):3797-807.
- Chen FU, Li Z, Zou L-F, Ma W-J, Li J-W, Chen Z, et al. Tribological behavior and mechanism of h-BN modified copper metal matrix composites paired with C/C-SiC. Tribol Int. 2021;153:106561.
- Zhao S, Zhang X, Zhong W, Wen Y, Yan Q. The wet braking and recovery behaviors of the P/M pad mated with C/C-SiC disc for high-speed trains. Wear. 2021;468-9. 203609.
- Zhao S, Yan Q, Peng T, Zhang X, Wen Y. The braking behaviors of Cu-Based powder metallurgy brake pads mated with C/C-SiC disk for high-speed train. Wear. 2020;448-9. 203237.
- Paris J-Y, Vincent L, Denape J. High-speed tribological behaviour of a carbon/silicon-carbide composite. Compos Sci Technol. 2001;61(3):417-23.
- Lu Y-H, Li Z, Zhou W, Xiao P. Manufacture and tribological behavior of C/C-SiC brake composites modified with Fe-Si alloy. J Ceramic Sci Technol. 2017;02:213-22.
- Hirsch PB, Roberts SG. The brittle-ductile transition in silicon. Philos Mag A. 1991;64(1):55-80.
- Liu Q, Huang G, Xu X, Fang C, Cui C. A study on the surface grinding of 2D C/SiC composites. Int J Adv Manuf Technol. 2017;93(5-8):1595-603.
- Wang D, Lu S, Xu D, Zhang Y. Research on material removal mechanism of C/SiC composites in ultrasound vibration-assisted grinding. Materials (Basel). 2020;13(8):1918.
- Xiao C-F, Grinding HB. Machining morphological studies on C/SiC composites. J Inst Eng India Ser D. 2018;99(2):209-15.

**How to cite this article:** Opel T, Langhof N, Krenkel W. Development and tribological studies of a novel metal-ceramic hybrid brake disc. Int J Appl Ceram Technol. 2022;19:62-74. <https://doi.org/10.1111/ijac.13826>